



**HAL**  
open science

## Self-potential signals induced by periodic pumping tests

Alexis Maineult, Elmar Strobach, Jörg Renner

► **To cite this version:**

Alexis Maineult, Elmar Strobach, Jörg Renner. Self-potential signals induced by periodic pumping tests. *Journal of Geophysical Research: Solid Earth*, 2008, 113, 10.1029/2007JB005193. insu-03603736

**HAL Id: insu-03603736**

**<https://insu.hal.science/insu-03603736>**

Submitted on 10 Mar 2022

**HAL** is a multi-disciplinary open access archive for the deposit and dissemination of scientific research documents, whether they are published or not. The documents may come from teaching and research institutions in France or abroad, or from public or private research centers.

L'archive ouverte pluridisciplinaire **HAL**, est destinée au dépôt et à la diffusion de documents scientifiques de niveau recherche, publiés ou non, émanant des établissements d'enseignement et de recherche français ou étrangers, des laboratoires publics ou privés.

Copyright

## Self-potential signals induced by periodic pumping tests

Alexis Maineult,<sup>1,2</sup> Elmar Strobach,<sup>1</sup> and Jörg Renner<sup>1</sup>

Received 30 May 2007; revised 9 October 2007; accepted 22 October 2007; published 16 January 2008.

[1] We measured the variations of the self-potential (SP) during periodic pumping tests performed at a test site located near a freshwater reservoir (Kemnader See, Bochum, Germany). Successions of injection and production intervals were applied in a borehole penetrating a jointed sandstone aquifer. We report the SP observations for tests with periods ranging between 10 and 60 min and flow rates between 10 and 25 L min<sup>-1</sup>. The SP responses at the surface exhibit the imposed period but are not truly harmonic contrary to the hydraulic pressure and SP measured in monitoring wells. In the grassy zone around the injection well, the amplitude of the SP signals decreases with distance from the injection well (around one order of magnitude at 10 m) in rough agreement with predictions for radial flow in a homogeneous medium around an infinite source. The shape of the SP responses also evolves with distance. Fourier spectral analysis reveals that the surface signals generally contain two main components at the main period and at half the period with the relative weight of the subperiodic components increasing with distance. Furthermore, the characteristics of the SP responses depend on whether the boreholes are left open or closed by packers. The comparison between surface and borehole measurements suggests that nonlinear phenomena are acting, probably related to the saturation and desaturation processes occurring in the vadose zone.

**Citation:** Maineult, A., E. Strobach, and J. Renner (2008), Self-potential signals induced by periodic pumping tests, *J. Geophys. Res.*, 113, B01203, doi:10.1029/2007JB005193.

### 1. Introduction

[2] Determining the hydraulic properties of the subsurface is fundamental for water resource management and oil and gas production. Reservoir transmissivity and storativity are usually estimated from pumping tests relying on observations of flow and pressure in the pumping well and pressure in monitoring wells [e.g., Horne, 1995; Fetter, 2001]. These classical tests have limitations regarding the characterization of local heterogeneities. First, the analysis is often based on the assumption of a homogeneous subsurface, at least beyond a certain length scale [Dagan, 1986; Gelhar, 1986]. Second, the large size of the investigated radius can lead to an averaging of the effects of heterogeneities [Sanchez-Vila et al., 1999]. Because heterogeneities can trigger flow channeling or conversely constitute barriers [e.g., Chandler et al., 1989; Bernabé and Bruderer, 1998], it is crucial to design new methodologies aimed at evidencing them, such as periodic pumping tests [Kuo, 1972; Hollaender et al., 2002; Rasmussen et al., 2003; Coptý and Findikakis, 2004; Renner and Messar, 2006]. The periodic operation limits the amount of fluid pumped and minimizes the perturbations of the system, as eventually

the mass balance is equal to zero [Rasmussen et al., 2003]. The analysis of flow and pressure at different periods, injection flow rates, and distances to the pumping well permits estimating spatial variations of hydraulic properties or at least indicates deviations from a homogeneous model [Coptý and Findikakis, 2004; Renner and Messar, 2006].

[3] To provide detailed information, classical pumping tests would require a certain number of wells, but the multiwell methods recently developed [e.g., Audouin and Bodin, 2007; Delay et al., 2007] are not applied in routine yet. Indeed, because of the high cost of drilling the areas of interest are generally sparsely covered. Apart from cost issues, an invasive strategy may be discarded owing to environmental risks and concerns regarding the effect of dense drilling on aquifer properties. Geophysical methods, such as geoelectrical prospecting, ground-penetrating radar, or self-potential (SP) monitoring, can complement hydraulic campaigns [e.g., Fetter, 2001] since they can be implemented over a large region with dense sampling in both space and time. SP monitoring is particularly appropriate to gather information on temporal variations in groundwater characteristics because it is directly sensitive to changes in flow or chemistry [e.g., Nourbehecht, 1963; Corwin and Hoover, 1979; Maineult et al., 2005; Revil and Linde, 2006]. In the absence of thermal and concentration gradients the electric potential  $U$  results from hydraulic flow only and is related to the hydraulic pressure  $p$  by the conservation law [e.g., Sailhac et al., 2003]

$$\nabla \cdot (\sigma \nabla U) = \nabla \cdot (\sigma C \nabla p), \quad (1)$$

<sup>1</sup>Institut für Geologie, Mineralogie und Geophysik, Ruhr-Universität Bochum, Bochum, Germany.

<sup>2</sup>Now at Géomatériaux et Environnement, Institut de Physique du Globe de Paris, Centre National de la Recherche Scientifique and Université Paris VII–Denis Diderot, Paris, France.

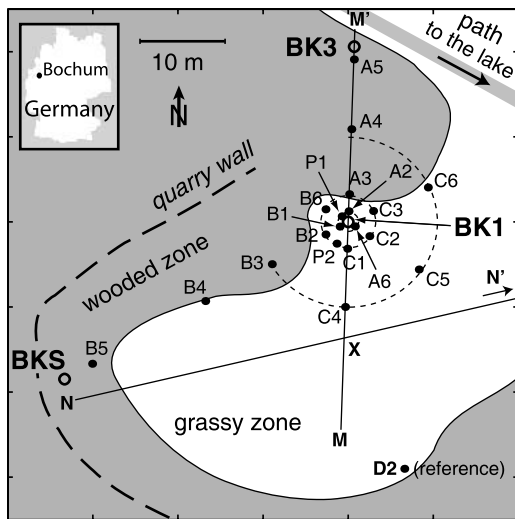


**Figure 1.** Test site map (Kemnader See, Bochum, Germany). Open circles are injection well (BK1) and observation wells (BK3 and BKS), solid circles are electrodes, and lines are the locations of the electrical pseudosections displayed in Figure 3.

where  $\sigma$  is the electrical conductivity of the saturated rock and  $C$  is the so-called electrokinetic coupling coefficient, possibly depending on the water saturation [e.g., *Revil and Cerepi*, 2004]. The hydraulic potential field is governed by the diffusion equation

$$S \frac{\partial p}{\partial t} = \nabla \cdot (K \nabla p), \quad (2)$$

where  $S$  is the specific storage and  $K$  is the hydraulic conductivity. The SP method has been used successfully to localize flow paths in the field [*Ogilvy et al.*, 1969; *Marquis et al.*, 2002; *Titov et al.*, 2002; *Revil et al.*, 2005; *Jardani et al.*, 2006; *Suski et al.*, 2006; *Linde et al.*, 2007a]. *Rizzo et al.* [2004] succeeded in quantitatively estimating the hydraulic conductivity of an aquifer from surface SP measurements during a pumping test, using a methodology validated in the laboratory [*Suski et al.*, 2004]. Numerical modeling [e.g., *Titov et al.*, 2005] and inversion [*Darnet et al.*, 2003; *Revil et al.*, 2003] are also available.

[4] Here we report on SP measurements during periodic pumping tests. Only few observations of natural periodic SP signals have been published to date. *Perrier and Morat* [2000] observed daily variations of about 1 mV in amplitude on 50-m dipoles, correlated with the soil temperature and resulting from capillary flow in the nonsaturated soil layer. *Zlotnicki and Le Mouél* [1990] explained the annual sinusoidal variations in the geomagnetic field at La Fournaise volcano by electrokinetic effects linked to rainfall cycles. *Trique et al.* [2002] studied the SP anomalies caused by the level variation of two connected lakes in the French Alps. *Perrier et al.* [1999, 2002] reported variations of 10 mV associated to a 30-min periodic spring in western Nepal. In both cases the correlation between the hydraulic sources and the SP signals was strongly evident, suggesting electrokinetic phenomena. *Kulessa et al.* [2003] concluded that the variations of SP measured beneath a glacier in Switzer-

land were forced by Earth and atmospheric tides. Note that at such frequencies (i.e., less than 0.01 Hz) no effects resulting from the frequency dependence of the electrokinetic coupling coefficient [*Reppert et al.*, 2001] are expected. Focusing on periodic signals may overcome notorious problems regarding the signal-to-noise ratio of SP measurements of small amplitudes (i.e., <10 mV), owing to telluric and anthropogenic electrical fields, plant activity, or temperature variations [*Petiau and Dupis*, 1980; *Clerc et al.*, 1998; *Gibert et al.*, 2006]. Indeed, signal processing tools such as Fourier transform can be employed successfully to eliminate variations with temporal characteristics differing from the excitation of interest.

## 2. Test Site and Procedure

### 2.1. Test Site

[5] The test site is located in a vacated sandstone quarry at the northwestern border of an artificial freshwater reservoir (Kemnader See) of the River Ruhr at the southern city limits of Bochum, Germany (Figure 1). The base of the quarry, bordered by a 15-m-high vertical wall at the east, was leveled with up to 4 m of mixed soil, clay, and pebbles. Below the surface layer the rock formation is made of thick layers of jointed, medium-grained, and coal-bearing sandstones embedding thin zones of siltstones. The sandstone, whose porosity ranges between 5 and 7%, is dissected by four joint orientations, one being parallel to the bedding [*Renner and Messar*, 2006].

[6] Three boreholes with a diameter of 10 cm penetrate the system (Figure 1); BK1 (30-m deep) and BK3 (20-m deep) are vertical, and BKS (32.1-m long) dips 60° southward perpendicularly to the bedding (Figure 2). Defining the reference level by the altitude of the surface at BK1, the ground surface is 0.75 m below reference at BK3 and 1.63 m above at BKS. Upper casings guarantee the stability of the section of the holes penetrating the landfill. The casings of BK1 (5-m long, top 73.5 cm above the ground surface) and BK3 (5.3 m long, top at 83.5 cm) are metallic, whereas BKS's casing is made of PVC (6.3 m long, top 10 cm above

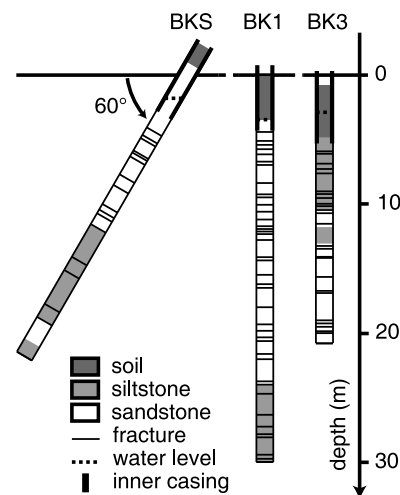


**Figure 2.** Simplified geologic stratigraphy derived from electrical resistivity logs and recovered cores (not at scale, that is, the diameter of the boreholes is 10 cm).

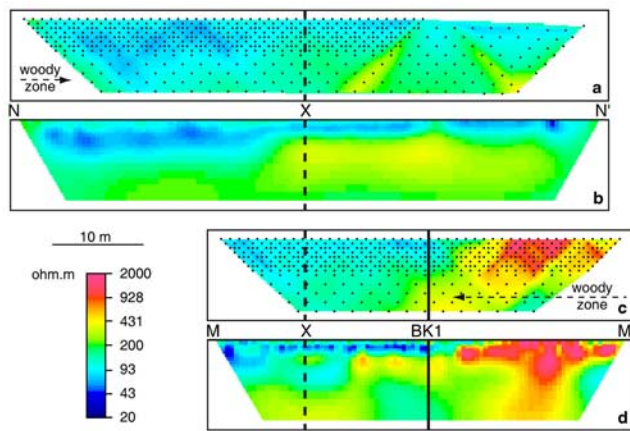


**Figure 3.** (a and c) Apparent resistivity and (b and d) 2-D-inverted resistivity of electrical pseudosections NN' and MM'.

the surface). The water table is approximately 3–3.5 m below the reference level.

[7] Electrical resistivity logs reveal that numerous joints cross the wells (Figure 2). Noticeably, a major steep fault crosses the BK1-BK3 line perpendicularly, as derived from outcrops and the lack of correlation between standard lithological logs (Figure 2). We also acquired electrical dipole-dipole pseudosections parallel and perpendicular to the direction NN' (Figure 1). The two-dimensional (2-D) resistivity distributions, inverted using DCIP2D software ([www.eos.ubc.ca/ubcgif/iag/sftwrdocs/dcip2d](http://www.eos.ubc.ca/ubcgif/iag/sftwrdocs/dcip2d)) with a root-mean-square error of 1% as stop criterion, evidence that the first meters in depth are rather homogeneous in the grassy zone (Figures 3a and 3b). In contrast, the electrical resistivity in the wooded zone is much higher (Figures 3c and 3d). In this area the resistive basement is surfacing and the thin soil layer, disturbed by the presence of numerous roots, pebbles, and stones, contains less moisture, all the more so the dense vegetation probably removes water. It also appears that the metallic casings do not perturb the resistivity distribution, at least at the scale of the employed dipole spacings of 1 and 2 m.

## 2.2. Periodic Pumping Tests

[8] We followed the methodology and used the equipment described by *Renner and Messar* [2006]. Contrary to classical pumping tests, which require the underground fluid being pumped continuously for a long time (i.e., step function in flow rate), a full harmonic test consists of  $N$  consecutive periods of duration  $T$ . A single period is defined by the following sequence, which yields a pressure signal in the pumping well resembling a sinusoidal variation [*Renner and Messar*, 2006]: injection in BK1 at constant flow rate  $Q_I$  during  $8T/30$ , no pumping for  $7T/30$ , production at constant flow rate  $Q_P$  during  $8T/30$ , and once again no pumping for  $7T/30$  (Figure 4a). First, freshwater from the reservoir (Kemnader See), previously stored in a barrel of 300 L, is injected. It is transferred from the barrel to BK1 through a flexible tube by means of an electrical suction pump coupled with a manifold permitting reversal of the

flow direction. The same volume is then removed from the aquifer to the barrel. The entire operation is repeated to obtain the desired number of periods. The mean flow rates  $Q_I$  and  $Q_P$  are deduced from the cumulative volume passed through the pump (measured with a volume meter placed at the entrance of the pump). In theory they must be equal to ensure no final perturbation of the water volume in the aquifer. Yet this condition is never satisfied exactly because the pump characteristics are asymmetric, i.e., the production from below the reference level is less effective than the injection. The pressure variations, directly proportional to the variations of the water level in the well (1 mbar  $\equiv$  1.02 cm H<sub>2</sub>O at 20°C), were monitored in the three wells at a sampling rate of 1 s with pressure loggers (Hope Hydrology), whose resolution is 0.1 mbar. Finally, for some tests we used packers to reduce the storage effect of the wells. We placed the packer 1.5 m below the normal water level in BK1 and 1 m below in BK3 and BKS. These depths ensured that wells would not fall dry below the packers during production, since the maximum variation of the water column in BK1 was about  $\pm 1.2$  m around the normal level.

## 2.3. Self-Potential Monitoring

[9] We recorded the electric potential differences (EPD) between measurement electrodes (denoted A2–A6, B1–B6, C1–C6, and P1 and P2) and the reference electrode D2 (Figure 1). The location of the latter ( $\sim 30$  m from BK1) was chosen a priori, assuming that here the potential would remain unaffected by the pumping operations. This permanently installed array allowed us to sample the potential along the lines BK1-BK3 and BK1-BKS and along three circles of approximately 1, 3, and 10 m in radius centered at BK1 (Figure 1). We used custom-made, unpolarizable Cu/CuSO<sub>4</sub> electrodes (26 cm in length, 4 cm in diameter, laboratory noise level of  $\pm 0.1$  mV), except P1 and P2, which were commercial Pb/PbCl<sub>2</sub> electrodes (SDEC PMS9000). Both types of electrodes were similar in terms of dynamics and intrinsic noise level. The electrodes were placed in 40-cm-deep holes filled up with a soil-bentonite-water mixture to ensure a good, permanent electrical contact [*Clerc et al.*, 1998] and covered with compacted soil. Note that these buried surface electrodes do not reach into the “source,” i.e., the excited, fully saturated aquifer. For some tests we submersed electrodes (denoted W1, W2, and WS) in the wells directly inside water to get an idea of the SP shape and amplitude in the fully saturated zone. Laboratory tests performed in a 3-m-high water column proved that our impermeable electrodes and the electrical connections are not damaged under water and that the readings are not pressure dependent.

[10] The electrodes were connected to a high-impedance ( $>10$  G $\Omega$ ) datalogger (Keithley model 2701) by means of coaxial cables, whose shields were all set at the same potential to reduce the effects of possible electromagnetic disturbances. The sampling rate for the potential measurements was 10 s (6 s for test 1, Table 1). Each EPD value was obtained by automatic averaging over 0.1 s. A delay of 0.4, 0.45, or 0.5 s, depending on the test, was applied before switching to the following channel to suppress the possible capacitance effects. Before analysis (particularly before applying the Fourier transform), each EPD was

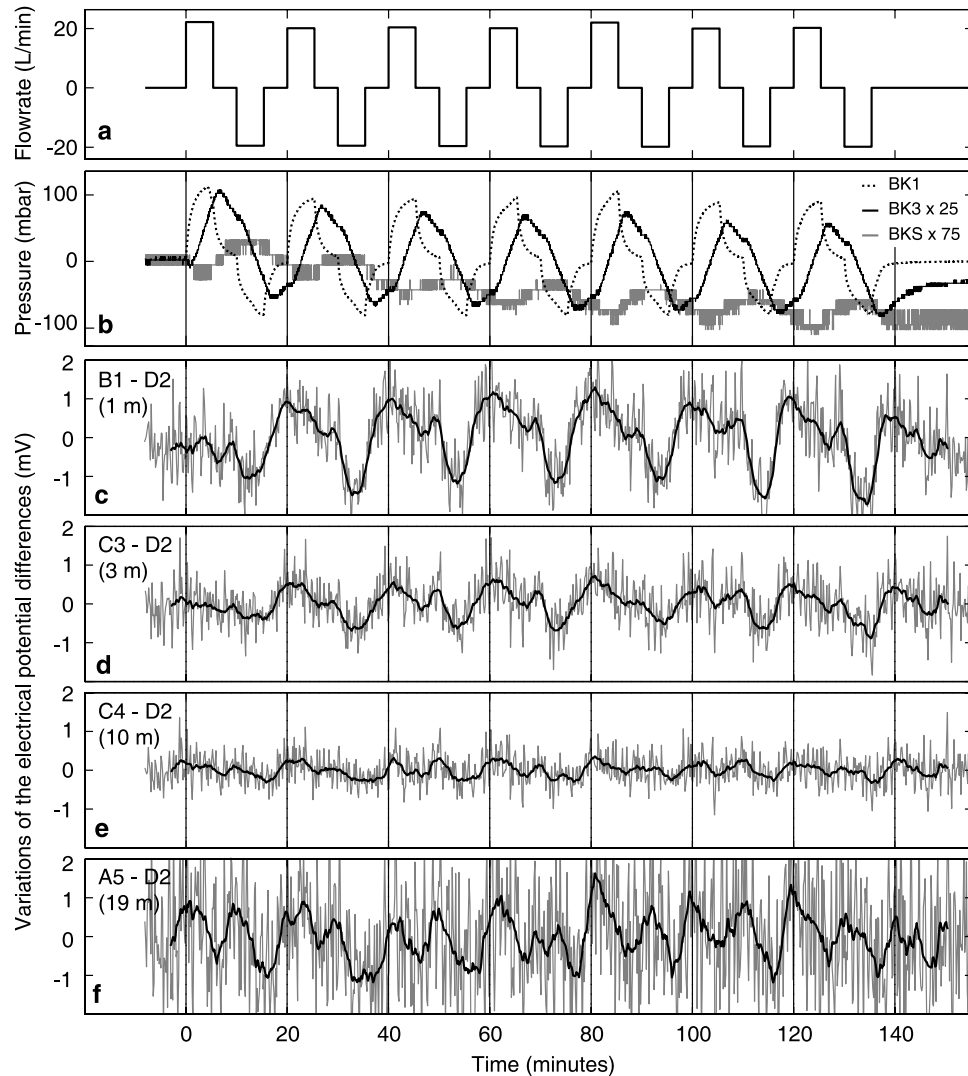


**Figure 4.** Example of records (test 7). (a) Mean injection flow rate observed at the pump and (b) pressure variations measured in the wells. Evolution of some detrended, electrical potential differences between electrodes at (c) 1, (d) 3, (e) 10 m from the injection well, and (f) near BK3 and the reference; grey lines are raw signals, and black lines are signals filtered using the second-order, Savitzky-Golay filter over a 5-min window. The vertical lines delimit the periods.

reduced by its individual, mean initial value and linearly detrended.

### 3. Observations

#### 3.1. Pressure Records

[11] Figure 4 presents the flow rate; the pressure variations in the boreholes and some electrical potential differences recorded during test 7 (Table 1) performed with open holes at a period of 20 min, an injection rate of  $20.7 \text{ L min}^{-1}$ , and a production rate of  $19.7 \text{ L min}^{-1}$  (Figure 4a). The evolution of the pressure in BK1 reflects a succession of symmetric loading-relaxation processes with peak-to-peak amplitude of about 200 mbar corresponding to water level variations of  $\pm 1$  m around the initial level (Figure 4b). The hydraulic “input function” in BK1, which includes the effect of the well storage capacity, triggers a roughly sinusoidal pressure response in the aquifer by diffusion, as observed in the monitoring wells (Figure 4b). The pressure field is charac-

terized by attenuation and phase shift increasing with distance (Figure 4b). The pressures in BK3 and BKS have also a low-frequency, slowly decreasing component. We do not think that this results from the double porosity of the system. Indeed, the pressure diffuses essentially in the highly permeable joints and the very low permeability of the sandstone (below  $10^{-17} \text{ m}^2$ ) strongly limits the penetration length inside the solid matrix at the involved timescales. The pressure variations for the other tests look similar with amplitudes increasing with flow rate and period (Table 1). Finally, in the case of packed wells the phase shift was smaller than in the case of open wells. This may result from the different hydraulic conditions in and near the injection well. The absence of well storage forces the water to circulate thus accelerating the propagation.

#### 3.2. SP Signals

[12] The raw SP data are dramatically noisy, yet periodicity can be seen with the naked eye for signals with

**Table 1.** Characteristics of the Tests

Test Wells	Period, min	Number of Periods	Mean Flow Rates, L min <sup>-1</sup>	BK1			BK3			BKS			BK1-BK3			BK1-BKS			Mean-Measured SP Amplitude, mV			D (m <sup>2</sup> s <sup>-1</sup> )/C <sub>app</sub> (V bar <sup>-1</sup> ) <sup>a</sup>
				Fourier Amplitude, mbar	Fourier Phase, deg	Periods for Pressure Analysis	Fourier Amplitude, mbar	Fourier Phase, deg	Periods for Pressure Analysis	Fourier Amplitude, mbar	Fourier Phase, deg	Periods for SP Analysis	D <sub>sp</sub> , m <sup>2</sup> s <sup>-1</sup>	D <sub>sp</sub> , m <sup>2</sup> s <sup>-1</sup>	D <sub>sp</sub> , m <sup>2</sup> s <sup>-1</sup>	At 1 m	At 3 m	At 10 m				
1 open	10	8	23.4 -19.7	64.2	-76.3	2-8	1.52	173.7	0.12	74.8	4-8	0.69	0.79	0.50	0.66	4-8	1.35	0.86	...	1.41/0.43 (0.92)	1.92/-0.022 (0.93)	
2 open	10	10	23.4 -19.7	64.4	-79.5	2-10	1.48	169.8	0.14	70.6	6-10	1.31	0.72	0.55	0.66	6-10	1.69	0.87	0.42	1.76/0.62 (0.96)	0.61/-0.030 (0.94)	
3 packers	10	9	20.1 -19.5	97.6	-63.7	2-9	2.88	-154.8	0.60	147.3	2-9	0.87	1.20	0.91	1.44	2-9	0.97	0.85	0.64	1.02/0.20 (0.58)	123.82/-0.009 (0.48)	
4 packers	10	7	23.9 -17.4	105.7	-63.6	2-7	3.04	-153.7	0.35	144.5	3-7	0.83	1.25	0.66	1.31	3-7	0.76	0.64	0.43	0.80/0.25 (0.78)	23.81/-0.007 (0.68)	
5 open	20	7	9.9 -9.9	35.5	-69.1	2-7	1.29	-143.7	0.12	121.8	4-7	0.55	0.99	0.26	0.57	4-7	1.39	0.85	0.46	1.45/0.50 (0.87)	1.23/-0.039 (0.86)	
6 open	20	7	17.7 -14.8	58.8	-71.2	2-7	1.60	-154.3	0.19	133.4	2-7	0.40	0.75	0.38	0.60	2-7	2.44	1.21	0.66	2.46/0.59 (0.97)	0.30/-0.047 (0.92)	
7 open	20	7	20.7 -19.7	73.2	-69.3	2-7	2.59	-145.0	0.21	127.7	2-7	0.55	0.95	0.27	0.57	2-7	2.39	1.36	0.52	2.76/0.69 (0.93)	0.32/-0.039 (0.96)	
8 open	20	7	23.2 -18.8	74.5	-68.5	2-7	2.64	-145.0	0.24	123.2	2-7	0.55	0.91	0.30	0.55	2-7	2.66	1.42	0.49	3.03/0.75 (0.94)	0.26/-0.042 (0.98)	
9 packers	20	8	19.4 -18.6	100.9	-60.4	2-8	3.96	-122.7	0.58	178.1	3-7	0.60	1.50	0.41	1.14	3-7	1.32	1.02	0.70	1.38/0.29 (0.71)	36.06/-0.011 (0.72)	
10 packers	20	6	23.7 -17.8	114.7	-59.5	2-6	4.27	-121.2	0.43	176.4	2-6	0.57	1.57	0.34	1.04	2-6	1.07	0.81	0.47	1.15/0.37 (0.73)	16.26/-0.008 (0.75)	
11 open	30	7	15.1 -15.1	58.7	-63.0	2-7	2.47	-122.7	0.22	150.6	2-6	0.46	1.10	0.22	0.48	2-6	2.32	1.26	0.67	2.36/0.56 (0.95)	0.39/-0.041 (0.93)	
12 open	60	4	15.0 -15.2	64.2	-59.1	2-4	3.29	-100.0	0.38	-164.4	2-4	0.32	1.58	0.33	0.15	2-4	3.43	1.91	0.92	3.70/0.60 (0.97)	0.17/-0.058 (0.96)	

<sup>a</sup>Values in parentheses are the adjustment coefficient.

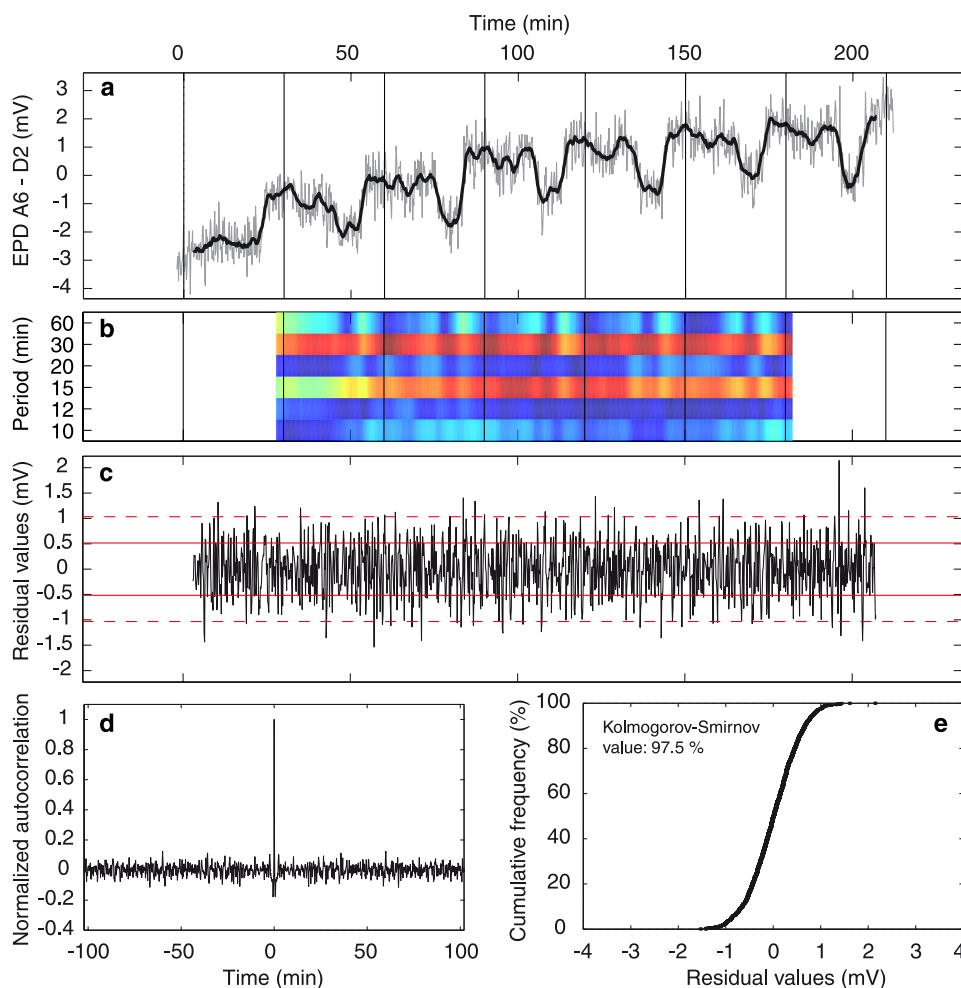


**Figure 5.** Example of filtering (test 11). (a) Raw signal, not detrended (grey) and signal filtered with the second-order Savitzky-Golay filter over a 5-min window (black). (b) Periodogram of the detrended, raw signal computed over a moving 60-min window. (c) Difference between raw and filtered signals (red lines are standard deviation values, and dotted red lines are double standard deviation values). (d) The Dirac-like autocorrelation and (e) the Gaussian distribution of the residue prove that the noise is white.

sufficient amplitude (an example is shown in Figures 4c–4f). For surface signals the strong attenuation with distance from the pumping well (Figures 4c–4f), close to one order of magnitude at a distance of 10 m, justifies the choice of D2 (~30 m from BK1, the injection well) as reference, since the perturbations near D2 are certainly negligible compared to those near the injection well. Therefore each detrended EPD can be considered as the “true” variations of the electrical potential at the considered measurement point.

### 3.2.1. Filtering

[13] For noise removal we applied the second-order Savitzky-Golay (SG) filter over a 5-min window. SG filtering prevents modifications of the amplitude and shift in the phase often produced by other filters when the signal contains very different frequencies [Press *et al.*, 1992]. The residual time series (differences between filtered and raw signals) for all the data have zero-centered, Dirac-like autocorrelations and a statistical distribution close to a perfect Gaussian curve with the Kolmogorov-Smirnov test value falling between 80 and 100% (note that the chosen 5-min window is optimal, since any change of this length introduces coherence in the autocorrelation and reduces the

Kolmogorov-Smirnov value). Thus the residues exhibit the characteristics of white Gaussian noise [e.g., *Mari et al.*, 1999]. As an example, Figure 5a shows the raw and filtered SP signal observed at the electrode A6 (1 m from BK1, Figure 1) during the 30-min periodic test 11 (Table 1). The residue (Figure 5c) exhibits an autocorrelation and a statistical distribution (Figures 5d and 5e) typical of white noise, and consequently the filtered signals can be viewed as close to the “real” ones. This notion is supported by the observation that the noise level NL of each EPD, estimated by the standard deviation of the residues and ranging between 0.2 and 1.3 mV, increases systematically with the length  $L$  of the dipole. The normalized quantity  $NL/L$  estimates the environmental noise level and ranges between 10 and 30  $\mu\text{V m}^{-1}$  with the higher value associated with the electrodes in the wooded zone.

### 3.2.2. SP Signals at the Surface

[14] The common characteristic features of SP signals recorded at the surface are described hereafter using test 7. The periodicity and the temporal coherence of the SP signals become obvious after filtering (Figures 4c–4f). At a distance of 1 m from BK1, significant SP variations are

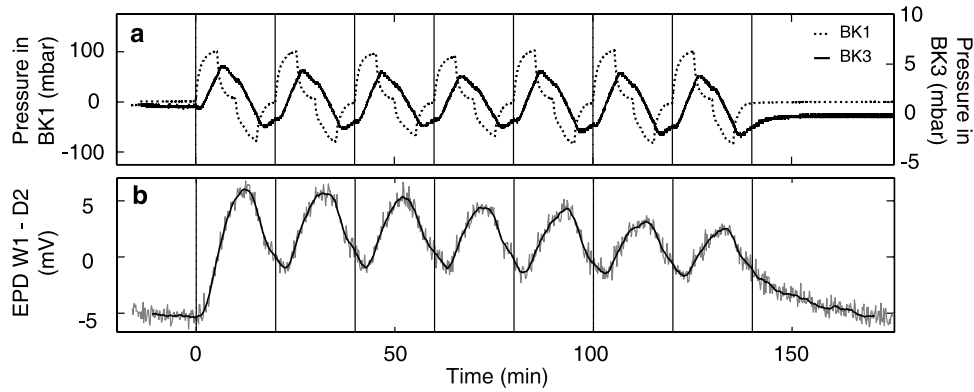


**Figure 6.** (a) Evolution of the pressure in the injection well BK1 and in the monitoring well BK3 during test 8. (b) Raw and filtered electrical potential difference between the electrode placed in the water column of BK1 and the reference.

observed already less than half a period after the start of the first injection (Figure 4c, B1). A characteristic period consists of an increase by slightly more than 2.0 mV in 7 min, followed by a quasi-linear decrease of about 1 mV in 8 min, a small increase of about 0.3 mV for 3 min, and finally a 1.8 mV sharp decrease. The shape of the signal at a distance of 3 m is similar, yet the amplitude is reduced by a factor slightly greater than 2 (Figure 4d, C3). The signal at 10 m is strongly attenuated for electrodes in the grassy area (Figure 4e, C4). Notably, not only the mean amplitude of the SP decreases but the shape is modified too. The signals clearly exhibit a period of 20 min but are not harmonic: They deviate from the sinusoid. Finally, note that the signals recorded at a given distance from BK1 in the grassy zone are coherent (they superimpose perfectly). In all tests the main shape of each SP signal is nonharmonic, constituted of a sharp increase, a slight decrease, and finally a small positive hump followed by a sharp decrease (compare Figures 4c, 4d, and 5a).

[15] To have a first look at the influence of the period, flow rate, and well configuration, we computed the mean value  $\Delta U_{m,n}$  of the peak-to-peak SP amplitudes for each period of every smoothed signal  $n$ . The averaged values  $\langle \Delta U_{m,n} \rangle$  at 1 ( $n = P1, A2, A6,$  and  $B1$ ), 3 ( $n = A3, B2, B6, C1, C2, C3,$  and  $P2$ ), and 10 m ( $n = C4, C5,$  and  $C6$ ) in the grassy zone are listed in Table 1. At given distance and flow rate the SP amplitude increases with period (compare test 11 to test 12, or test 1 and 2 to tests 6, 7, and 8). Similarly, for a given period the SP amplitude increases with flow rate (compare test 5 to test 6). This proves that the source of SP is electrokinetics: The higher the pressure in the injection well, the larger the SP (equation (1)). To roughly characterize the SP attenuation with distance, we assumed a power law such as  $\Delta U_{m,n} = A r_n^{-B}$ , where  $r_n$  is the distance between electrode  $n$  and BK1. We determined  $A$  and  $B$  by a least squares fitting procedure (Table 1). For the open pumping well the  $B$  value is around 0.6 (with an excellent adjustment coefficient  $r^2$ ) and seems to be relatively independent of period and flow rate. When a packer was placed in the pumping well, the amplitudes at 1 m are lower than for the open well, leading to a different, poorly determined  $B$  value (around 0.3). When packers are present, there is probably less vertical fluid movement in the vicinity of the

injection well. The electrical source is thus deeper and the surface signal smaller.

[16] The signals recorded in the wooded zone (electrodes A4, A5, B3, B4, and B5) are extremely noisy and often incoherent (Figure 4f, A5). The noise can result from a less efficient electrical contact due to the soil heterogeneity and lower-moisture content but also from biological noise or even from high contrasts in resistivity (Figure 3) inducing a high, local polarization. Unexpectedly, the SP amplitudes seem to increase slightly with distance to BK1. We do not think that the well's casings trigger such a behavior [e.g., *Schenkel and Morrison, 1990*], as (1) BKS's casing is made of plastic, (2) no spatial SP anomalies were observed at equilibrium (i.e., without any flow), and (3) the electrical pseudosections do not evidence any perturbation of conductivity around the wells (Figure 3). An alternative explanation could be a local change in pressure gradient resulting in a local increase of the electrokinetic response, for example, related to drilling-induced damage in the vicinity of the observation wells. However, the cause could also simply be a variation in the electrical properties of the subsurface, i.e., in the rock conductivity  $\sigma$  or in the coupling coefficient  $C$  (equation (1)), which evolve toward the quarry wall and near the coal vein outcropping in the vicinity of BK3 (Figure 3). The expanded form of equation (1)

$$\nabla \cdot \nabla U + \frac{\nabla \sigma}{\sigma} \nabla U = C \nabla \cdot \nabla p + C \frac{\nabla \sigma}{\sigma} \nabla p + \nabla C \nabla p \quad (3)$$

underlines the influence of the  $\sigma$  and  $C$  gradients. For example, in the upper layer near the contact between the grassy and wooded zones the quantity  $\nabla \sigma / \sigma$  is certainly greater than  $0.1 \text{ m}^{-1}$  (Figure 3) and the second-order terms in equation (3) are no longer negligible.

### 3.2.3. SP Signals in Boreholes

[17] The SP signals recorded in the water column of BK1 are remarkably different from surface measurements, as shown in Figure 6 for the 20-min periodic test 8. The SP signal in BK1 exhibits a sinusoidal variation, whose amplitude slightly diminishes with time, superimposed to a linear decrease and to an offset with respect to the initial state (i.e., before the injection starts). Under the assumption that the well water is an electrical equipotential the SP signals recorded in the boreholes are representative of the SP field

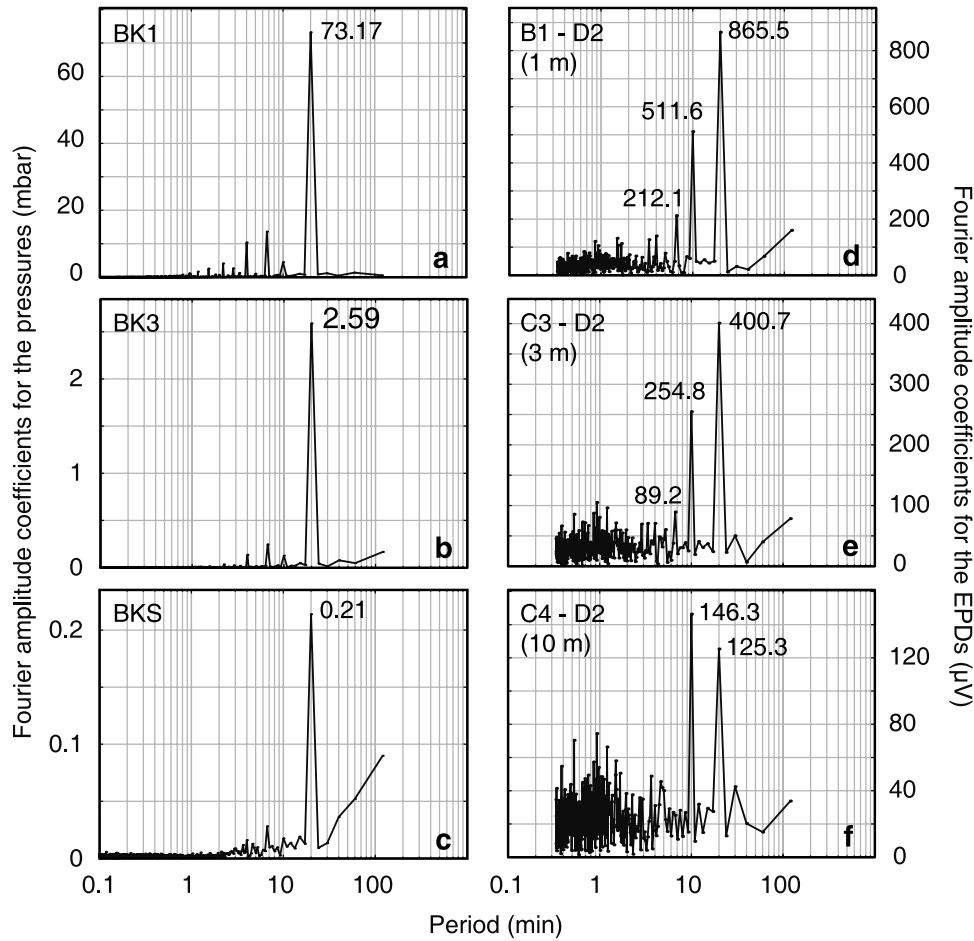


**Figure 7.** Fourier amplitude spectra for (a–c) the pressure and the (d–f) detrended, raw self-potential, corresponding to the time series shown in Figure 4 (test 7).

in the close vicinity of the wells inside the saturated zone. Unfortunately, the SP signals recorded in BK3 and BKS were too noisy to provide any valuable information.

## 4. Discussion

### 4.1. Estimates of the Hydraulic Properties From Pressure Records

[18] Pressure records obtained during periodic pumping tests are advantageously analyzed computing their Fourier transform [Renner and Messar, 2006]. Fourier spectra are similar for all tests and well exemplified by the amplitude spectra of test 7 (Figure 4b), computed over the last five periods to eliminate the initial transient part (Figures 7a–7c). A main peak is located at the imposed period  $T = 20$  min with amplitude coefficients of 73.2, 2.6, and 0.21 mbar for BK1, BK3 and BKS, respectively. Secondary peaks occur at  $T/2 = 10$ ,  $T/3 = 6.67$ , and  $T/4 = 4$  min, the peak at 10 min always being the smallest. Pressure recorded thus also deviates from sinusoid, but the deviation is very small and diminishes significantly with distance as the diffusion phenomenon acts as a low-pass filter.

[19] The quantitative interpretation of attenuation and phase shift requires an a priori model. The simplest is the

two-dimensional, infinite, homogeneous, confined aquifer, for which the pressure equation (2) becomes

$$\frac{1}{D} \frac{\partial p}{\partial t} = \frac{\partial^2 p}{\partial r^2} + \frac{1}{r} \frac{\partial p}{\partial r}, \quad (4)$$

where  $D$  denotes aquifer diffusivity ( $K/S$  ratio) and  $t$  denotes time. Applying a sinusoidal boundary condition in time at the wall of the injection well (of radius  $r_0$ ), the theoretical attenuation  $\delta p$  and phase shift  $\delta \varphi$  are given by [Renner and Messar, 2006]

$$\delta p(r) = \frac{\Delta p(r)}{\Delta p(r_0)} = \left| \frac{K_0(\eta r)}{K_0(\eta r_0)} \right|, \quad (5)$$

where  $\Delta p(r)$  is the peak-to-peak amplitude at distance  $r$ , and

$$\delta \varphi(r) = \arg \left( \frac{K_0(\eta r)}{K_0(\eta r_0)} \right). \quad (6)$$

$K_0$  is the second-kind Bessel function of zeroth-order. The parameter  $\eta$  relates to period  $T$  by

$$\eta = \sqrt{i \frac{2\pi}{DT}}. \quad (7)$$

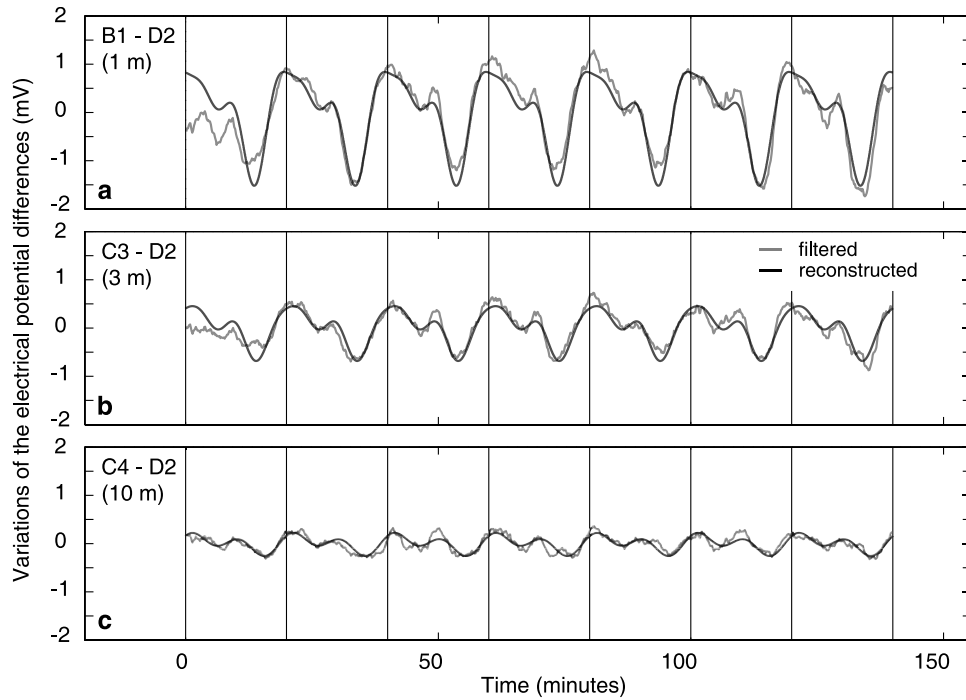


**Figure 8.** Detrended SP signals filtered (grey) and reconstructed from the main components of the Fourier spectra (black), corresponding to the data shown in Figures 4 and 7 (test 7).

[20] The diffusivity values  $D_{\delta p}$  inferred from equation (5) and  $D_{\delta \phi}$  from equation (6) using the main Fourier amplitude and phase coefficients for the two couples BK1-BK3 and BK1-BKS are consistently around  $0.5 \text{ m}^2 \text{ s}^{-1}$  (Table 1) in agreement with the values previously determined by *Renner and Messar* [2006]. Though close,  $D_{\delta p}$  and  $D_{\delta \phi}$  are not strictly equal, indicating that the model used for the interpretation is not adequate (in particular, the real medium is finite and heterogeneous, and the upper boundary is free). Interestingly,  $D_{\delta \phi}$  is strongly dependent on the presence or absence of packers in the pumping well, its value being three times higher when packers are used. This point, not investigated by *Renner and Messar* [2006], underlines the need for further refined models taking into account the effects of the storage capacity of the injection well and even vertical movement in its vicinity.

## 4.2. Relation Between Fluid Flow and Evolution of SP Signals With Distance

### 4.2.1. Spectral Analysis of SP Signals

[21] As for pressure records, we computed the Fourier spectra for the linearly detrended but unfiltered SP variations. For example, the Fourier analysis of the SP signal observed at the electrode A6 (1 m from BK1, Figure 1) during the 30-min periodic test 11 (Table 1) carried out using a 60-min-wide moving window evidences its periodicity with major contributions of the 30- and 15-min components to the amplitude (Figure 5b). The presence of two main periods reveals the nonharmonicity of the SP response. Note that we did not use the transient, initial part of the SP signals (evidenced by the periodograms, as shown in Figure 5b) for the analysis (Table 1). For all tests we observed spectral features similar to the ones displayed for test 7 (Figures 7d–7f, corresponding to the signals of

Figures 4c–4e). The electrodes at 1 and 3 m from the pumping well (except A3) exhibit three main peaks at  $T = 20$ ,  $T/2 = 10$ , and  $T/3 = 6.67$  min (Figures 7d and 7e). The third peak at 6.67 min is not present or masked by the noise for the more distant electrodes (Figure 7f). The change in signal shape with distance is reflected by the increase in the ratio  $a_{10}/a_{20}$  from 0.6 at 1 m to up to 2 at 10 m, where  $a_{20}$  and  $a_{10}$  denote the Fourier amplitude coefficients at 20 and 10 min respectively. We attempted to reconstruct an “average signal” over a period from the spectra as

$$U_r(t) = \sum_{j=\{T, T/2, T/3, \dots\}} a_j \cos\left(\frac{2\pi}{j}t + \varphi_j\right) \quad t \in [0, T], \quad (8)$$

where  $a_j$  and  $\varphi_j$  are the SP Fourier amplitude and phase coefficients at the  $j$ th period. The reconstructed signals are remarkably similar to the smoothed signals (Figures 8a–8c) but free of statistical variations. Peak-to-peak amplitudes of the reconstructed signals  $\Delta U_r$  are only a little smaller than the mean amplitudes  $\Delta U_m$  (Figures 9e and 9f), demonstrating that the main part of the energy is concentrated in the three considered spectrum components. SP signals for tests with packered pumping well exhibit less dependence on distance in Fourier amplitude ( $a_{10}$ ,  $a_5$ , and  $a_{3.33}$ ) and phase coefficients ( $\varphi_{10}$ ,  $\varphi_5$ , and  $\varphi_{3.33}$ ) than signals recorded for pumping tests in an open hole configuration (Figure 9). This is possibly related to the fact that the amplitude of the variations of the water level is smaller in the vicinity of the injection well when it is packered.

### 4.2.2. Estimation of Hydraulic Properties From Observed SP Signals

[22] In our tests, electrodes are placed in the soil and gravel layer with a thickness of  $\sim 4$  m covering the

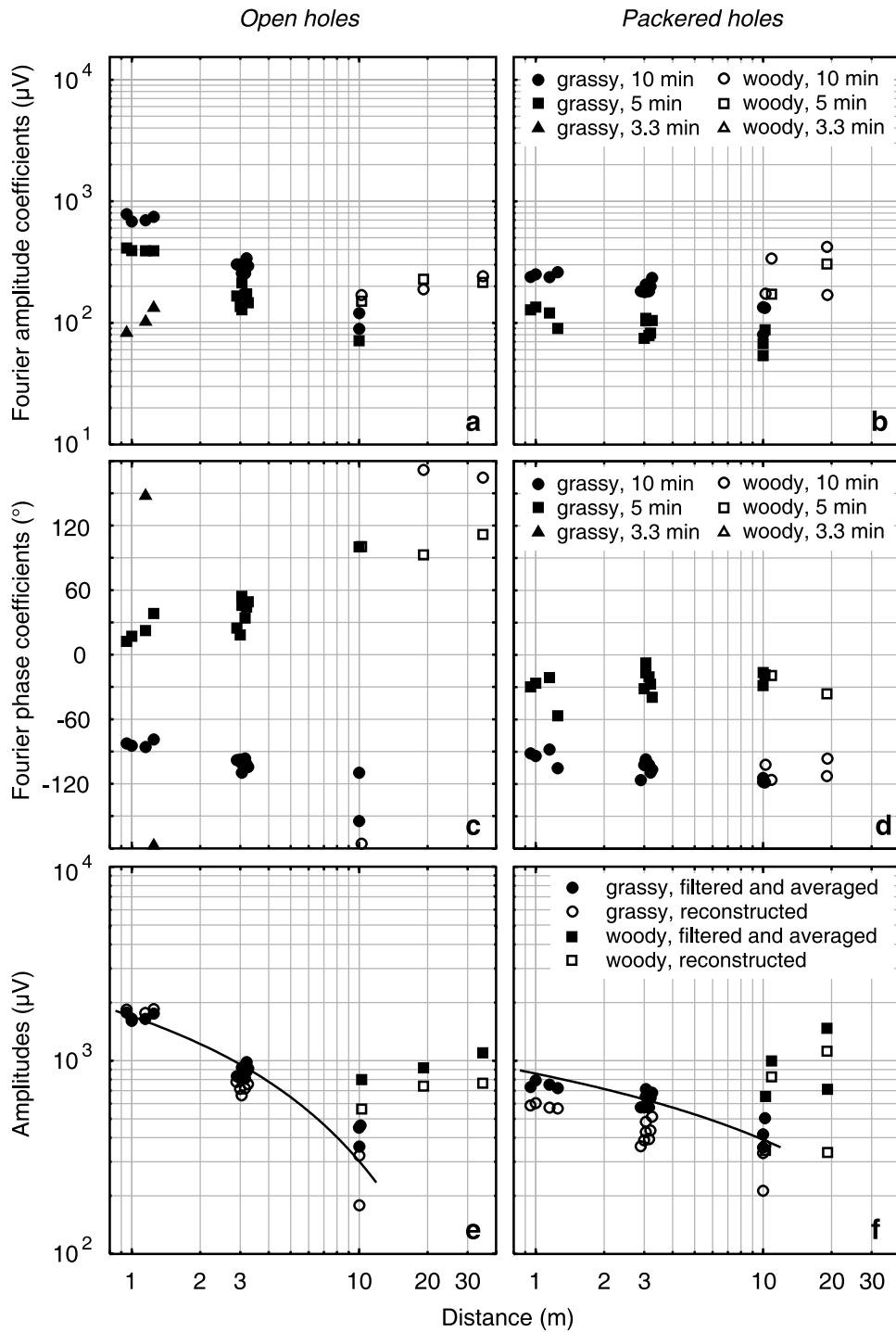


**Figure 9.** Evolution of the Fourier amplitude coefficients  $a_{10}$ ,  $a_5$  and  $a_{3.3}$  for (a) the tests 2 and (b) 4. (c and d) Corresponding Fourier phase coefficients  $\phi_{10}$ ,  $\phi_5$ , and  $\phi_{3.3}$ . (e and f) Corresponding mean measured amplitude  $\Delta U_m$  and reconstructed amplitude  $\Delta U_r$  with respect to the distance to the injection well and empirical curve computed on  $\Delta U_m$  using equation (10). See section 4.2.

sandstone formation. The natural water level is below the corresponding interface. Thus we have to distinguish electrical fields in the saturated zone composing the aquifer in which water movement occurs and in the dry top layer housing the electrodes. In addition, the vadose zone and its temporal variations during periodic pumping tests (in terms of extension and water content) may alter electrical fields.

[23] First, we address the alteration that the electric field associated with the streaming potential in the aquifer experiences in the dry top layer. The phase and attenuation constants  $\alpha$  and  $\beta$  experienced by an electromagnetic wave  $\mathbf{E} = \mathbf{E}_0 \exp(-i\alpha z) \exp(-\beta z) \exp(2\pi i t/T)$ , which propagates along the  $z$  direction through a medium characterized by dielectric permittivity  $\epsilon$  and magnetic permeability  $\mu$ , are

strongly frequency dependent [e.g., Zonge and Hughes, 1991]. Assuming  $\mu = \mu_0$ , for the encountered range in rock conductivity ( $2\text{--}20 \text{ mS m}^{-1}$ ), a reasonable range in relative dielectric permittivity for soils and rocks of  $10\text{--}40$ , and the employed periods ( $10\text{--}60 \text{ min}$ ), these coefficients are negligible, less than  $1.1 \cdot 10^{-5} \text{ m}^{-1}$ . It is important to note that the employed pumping periods are huge even compared to time intervals of pole inversion of nominal DC methods ( $\sim 1 \text{ s}$ ) employed to minimize polarization effects.

[24] At steady state conditions the interpretation of the SP signals in terms of pressure field is based on the judicious use of equation (1). The electrical potential should preserve the shape of the hydraulic input function in the saturated zone, even if this function is time dependent. Indeed, the electrode placed in the injection borehole recorded unshifted sinusoidal variations (Figure 6).

[25] For an unconfined, homogeneous aquifer the pressure at point  $x$  can be related at the first order to the surface self-potential by [Linde *et al.*, 2007a]

$$p(x) - p(x_0) = \frac{U(x) - U(x_0)}{C_s - C_v}, \quad (9)$$

where  $x_0$  is a reference point.  $C_s$  and  $C_v$  are the coupling coefficients in the saturated and vadose zones, respectively.  $C_s$  is constant, whereas  $C_v$  depends on the rock saturation  $S$  [Guichet *et al.*, 2003; Revil and Cerepi, 2004]. When the water table undergoes temporal variations, saturation and desaturation processes occur in the unsaturated zone. Because these processes are asymmetric [Mualem, 1974] and the dependence of  $C_v$  on saturation is nonlinear [Linde *et al.*, 2007b; Revil *et al.*, 2007], the surface self-potential is no longer proportional to the pressure, probably explaining the phase shift we observed between pressure and SP (Figure 4) and the splitting of the energy (Figure 7). The asymmetric shape of the SP response (Figures 4 and 8) is in agreement with the theoretical assessment by Linde *et al.* [2007b] and Revil *et al.* [2007] that predicts a hysteretic response of SP to saturation-desaturation cycles.

[26] Consequently, determining diffusivity from our SP data is not straightforward. In particular, it would require the knowledge of the relation  $C_v(S)$  and even a model of the piezometric variations induced by a sinusoidal excitation. For a zeroth-order estimate we can assume that SP and pressure signals are similarly attenuated with distance. So, by combining equations (5) and (9) we obtain

$$\Delta U(r) = |C_{app}| \Delta p(r_0) \left| \frac{K_0(\eta r)}{K_0(\eta r_0)} \right|, \quad (10)$$

where  $C_{app}$  is an apparent coupling coefficient. We searched the optimal parameters  $D$  in the range  $[0.01, 200] \text{ m}^2 \text{ s}^{-1}$  and  $C_{app}$  in  $[-0.001, -0.1] \text{ V bar}^{-1}$  in the least squares sense for the averaged amplitudes  $\Delta U_{m,n}$  in the grassy zone and a peak-to-peak pressure amplitude  $\Delta p(r_0)$  equal to twice the main Fourier amplitude coefficient (Table 1 and Figures 9e and 9f). The diffusivities so obtained are in agreement with the values determined from pressure analysis in the case of open holes (i.e.,  $D \approx 0.1\text{--}1 \text{ m}^2 \text{ s}^{-1}$ , Table 1). The absolute value of the apparent coupling coefficient is around  $0.04 \text{ V bar}^{-1}$ , consistent with the values reported by Linde *et al.* [2007a, 2007b]. For the

packed pumping well the diffusivity values are significantly higher and the apparent coefficient smaller than above values. Only a refinement of this crude approach combined with laboratory measurements could help to determine the diffusivity properly.

## 5. Concluding Statements

[27] We showed that SP signals acquired during periodic pumping tests, even weak and noisy, contain valuable information, provided that an adequate filtering and spectral analysis are applied. The characteristics of the SP signals clearly correlate with the pressure field in the subsurface, i.e., they are periodic, attenuated, and phase shifted with distance. At zeroth order it seems that the attenuation of SP amplitude with distance is similar to the pressure attenuation and thus that hydraulic diffusivity could be inferred from SP. Furthermore, the shape of the surface SP signals deviate more from a harmonic function than observed pressures, indicating that the relationship between hydraulics and electrics is not linear. The comparison between surface and borehole measurements suggests also that saturation and desaturation processes play a major role. The deviation from harmonic signals may thus be a clue to vadose zone properties.

[28] New field measurements with a denser sampling in space; detailed hydrological modeling of the aquifer system, including the vadose zone; and application of Linde *et al.*'s [2007b] and Revil *et al.*'s [2007] theory for the modeling of the electrokinetic response to saturation-desaturation will be required for further interpretation of our data. Studying the evolution of SP during saturation-desaturation and reproducing the periodic pumping in the laboratory could also help to enlighten the open issues.

[29] **Acknowledgments.** This study was generously supported by the German Science Foundation (SFB 526 "Rheology of the Earth"). We thank F. Z. Z. Kemnade GmbH for free access to the site, F. Bettenstedt and M. Messar for assistance in the field, M. Zamora (Institut de Physique du Globe Paris) for providing the Pb/PbCl<sub>2</sub> electrodes, and M. Degutsch (Westfälische Wilhelms-Universität Münster) for lending us a multielectrode Syscal resistivity meter. We are also grateful to Associate Editor A. Revil, L. Slater, and an anonymous reviewer for their constructive comments and N. Linde and F. Perrier for fruitful discussions. This is IPG contribution 2277.

## References

- Audouin, O., and J. Bodin (2007), Analysis of slug-tests with high-frequency oscillations, *J. Hydrol.*, *334*, 282–289.
- Bernabé, Y., and C. Bruderer (1998), Effect of the variance of pore size distribution on the transport properties of heterogeneous networks, *J. Geophys. Res.*, *103*(B1), 513–525.
- Chandler, M. A., G. Kocurek, D. J. Coggin, and L. W. Lake (1989), Effects of stratigraphic heterogeneity on permeability in eolian sandstone sequence, Page Sandstone, northern Arizona, *AAPG Bull.*, *73*, 658–668.
- Clerc, G., G. Petiau, and F. Perrier (Eds.) (1998), The Garchy 1995–1996 electrode experiment, technical report, Comm. à l'Energ. At., Bruyères-le-Châtel, France.
- Coppy, N. K., and A. N. Findikakis (2004), Stochastic analysis of pumping test drawdown data in heterogeneous geologic formation, *J. Hydraul. Res.*, *42*, 59–67.
- Corwin, R. F., and D. B. Hoover (1979), The self-potential method in geothermal exploration, *Geophysics*, *44*, 226–245.
- Dagan, G. (1986), Statistical theory of groundwater flow and transport: Pore to laboratory, laboratory to formation, and formation to regional scale, *Water Resour. Res.*, *22*, 121–135.
- Darnet, M., G. Marquis, and P. Sailhac (2003), Estimating aquifer hydraulic properties from the inversion of surface streaming-potential (SP) anomalies, *Geophys. Res. Lett.*, *30*(13), 1679, doi:10.1029/2003GL017631.

- Delay, F., A. Kaczmaryk, and P. Ackerer (2007), Inversion of interference hydraulic pumping tests in both homogeneous and fractal dual media, *Adv. Water Resour.*, *30*, 314–334.
- Fetter, C. W. (2001), *Applied Hydrogeology*, 4th ed., 298 pp., Macmillan, New York.
- Gelhar, L. W. (1986), Stochastic subsurface hydrology from theory to application, *Water Resour. Res.*, *22*, 135–145.
- Gibert, D., J. L. Le Mouél, L. Lambs, F. Nicollin, and F. Perrier (2006), Sap flow and daily electric potential variations in a tree trunk, *Plant Sci.*, *171*, 572–584.
- Guichet, X., L. Jouniaux, and J. P. Pozzi (2003), Streaming potential of a sand column in partial saturation conditions, *J. Geophys. Res.*, *108*(B3), 2141, doi:10.1029/2001JB001517.
- Hollaender, F., P. Hammond, and A. C. Gringarten (2002), Harmonic testing for continuous well and reservoir monitoring, paper SPE 77692 presented at SPE Annual Technical Conference and Exhibition, Soc. of Pet. Eng., San Antonio, Tex.
- Home, R. N. (1995), *Modern Well Test Analysis*, 2nd ed., 257 pp., Petro- way, Palo Alto, Calif.
- Jardani, A., J. P. Dupond, and A. Revil (2006), Self-potential signals with preferential groundwater flow pathways in sinkholes, *J. Geophys. Res.*, *111*, B09204, doi:10.1029/2005JB004231.
- Kullessa, B., B. Hubbard, G. H. Brown, and J. Becker (2003), Earth tide forcing of glacier drainage, *Geophys. Res. Lett.*, *30*(1), 1011, doi:10.1029/2002GL015303.
- Kuo, C. H. (1972), Determination of reservoir properties from sinusoidal and multirate flow tests in one or more wells, *Soc. Pet. Eng. J.*, *12*, 499–506.
- Linde, N., A. Revil, A. Bolève, C. Dagès, J. Castermant, B. Suski, and M. Voltz (2007a), Estimation of the water table throughout a catchment using self-potential and piezometric data in a Bayesian framework, *J. Hydrol.*, *334*, 88–98.
- Linde, N., D. Jougnot, A. Revil, S. K. Matthäi, T. Arora, D. Renard, and C. Doussan (2007b), Streaming current generation in two-phase flow conditions, *Geophys. Res. Lett.*, *34*, L03306, doi:10.1029/2006GL028878.
- Maineult, A., Y. Bernabé, and P. Ackerer (2005), Detection of advected concentration and pH fronts from spontaneous potential measurements, *J. Geophys. Res.*, *110*, B11205, doi:10.1029/2005JB003824.
- Mari, J. L., F. Glangeaud, and F. Coppens (1999), *Signal Processing for Geologists and Geophysicists*, 458 pp., Technip, Paris.
- Marquis, G., M. Darnet, P. Sailhac, A. K. Singh, and A. Gérard (2002), Surface electric variations induced by deep hydraulic stimulation: An example from the Soutz HDR site, *Geophys. Res. Lett.*, *29*(14), 1662, doi:10.1029/2002GL015046.
- Mualem, Y. (1974), A conceptual model of hysteresis, *Water Resour. Res.*, *10*, 514–520.
- Nourbehecht, B. (1963), Irreversible thermodynamic effects in inhomogeneous media and their applications in certain geoelectric problems, Ph.D. thesis, Mass. Inst. of Technol., Cambridge.
- Ogilvy, A. A., M. A. Ayed, and V. A. Bogoslovsky (1969), Geophysical studies of water leakages from reservoirs, *Geophys. Prospect.*, *17*, 36–62.
- Perrier, F., and P. Morat (2000), Characterization of electrical daily variations induced by capillary flow in the non-saturated zone, *Pure Appl. Geophys.*, *157*, 785–810.
- Perrier, F., M. Trique, J. Aupiais, U. Gautham, and P. Shrestha (1999), Electric potential variations associated with periodic spring discharge in western Nepal, *C. R. Acad. Sci., Ser. IIA Sci. Terre Planetes*, *328*, 73–79.
- Perrier, F., U. Gautam, G. R. Chitrakar, P. Shrestha, B. Kafle, T. Héritier, and J. Aupiais (2002), Geological, geochemical and electrical constraints on the transient flow mechanism of the Dhor Barahi periodic spring in western Nepal, *J. Nepal Geol. Soc.*, *26*, 109–119.
- Petiau, G., and A. Dupis (1980), Noise, temperature coefficient, and long time stability of electrodes for telluric observations, *Geophys. Prospect.*, *28*, 792–804.
- Press, W. H., B. P. Flannery, S. A. Teukolsky, and W. T. Vetterling (1992), *Numerical Recipes in C: The Art of Scientific Computing*, 2nd ed., 994 pp., Cambridge Univ. Press, New York.
- Rasmussen, T. C., K. G. Haborak, and M. H. Young (2003), Estimating aquifer hydraulic properties using sinusoidal pumping at the Savannah River site, South Carolina, USA, *Hydrogeol. J.*, *11*, 466–482.
- Renner, J., and M. Messar (2006), Periodic pumping tests, *Geophys. J. Int.*, *167*, 479–493.
- Reppert, P. M., F. D. Morgan, D. P. Lesmes, and L. Jouniaux (2001), Frequency-dependent streaming potentials, *J. Colloid Interface Sci.*, *234*, 194–203.
- Revil, A., and A. Cerepi (2004), Streaming potentials in two-phase flow conditions, *Geophys. Res. Lett.*, *31*, L11605, doi:10.1029/2004GL020140.
- Revil, A., and N. Linde (2006), Chemico electro-mechanical coupling in microporous media, *J. Colloid Interface Sci.*, *302*, 682–694.
- Revil, A., V. Naudet, J. Nouzaret, and M. Pessel (2003), Principles of electrography applied to self-potential electrokinetic sources and hydrogeological applications, *Water Resour. Res.*, *39*(5), 1114, doi:10.1029/2001WR000916.
- Revil, A., L. Cary, Q. Fan, A. Finizola, and F. Trolard (2005), Self-potential signals associated with preferential ground water flow pathways in a buried paleo-channel, *Geophys. Res. Lett.*, *32*, L07401, doi:10.1029/2004GL022124.
- Revil, A., N. Linde, A. Cerepi, D. Jougnot, S. Matthäi, and S. Finsterle (2007), Electrokinetic coupling in unsaturated porous media, *J. Colloid Interface Sci.*, *313*, 315–327.
- Rizzo, E., B. Suski, A. Revil, S. Straface, and S. Troisi (2004), Self-potential signals associated with pumping tests experiments, *J. Geophys. Res.*, *109*, B10203, doi:10.1029/2004JB003049.
- Sailhac, P., M. Darnet, and G. Marquis (2003), Electrical streaming potential measured at the ground surface: Forward modeling and inversion issues for monitoring infiltration and characterizing the vadose zone, *Vadose Zone J.*, *3*, 1200–1206.
- Sánchez-Vila, X., C. L. Axness, and J. Carrera (1999), Upscaling transmissivity under radially convergent flow in heterogeneous media, *Water Resour. Res.*, *35*, 613–621.
- Schenkel, C. J., and H. F. Morrison (1990), Effect of well casing on potential field measurements using downhole current sources, *Geophys. Prospect.*, *38*, 663–686.
- Suski, B., E. Rizzo, and A. Revil (2004), A sandbox experiment of self-potential signals associated with a pumping test, *Vadose Zone J.*, *3*, 1193–1199.
- Suski, B., A. Revil, K. Titov, P. Konosavsky, M. Voltz, C. Dagès, and O. Huttel (2006), Monitoring of an infiltration experiment using the self-potential method, *Water Resour. Res.*, *42*, W08418, doi:10.1029/2005WR004840.
- Titov, K., Y. Ilyin, P. Konosavski, and A. Levitsky (2002), Electrokinetic spontaneous polarization in porous media: Petrophysics and numerical modelling, *J. Hydrol.*, *267*, 207–216.
- Titov, K., A. Revil, P. Konosavsky, S. Straface, and S. Troisi (2005), Numerical modeling of self-potential signals associated with a pumping test experiment, *Geophys. J. Int.*, *162*, 641–650.
- Trique, M., F. Perrier, T. Froidefond, J.-P. Avouac, and S. Hautot (2002), Fluid flow near reservoir lakes inferred from the spatial and temporal analysis of the electric potential, *J. Geophys. Res.*, *107*(B10), 2239, doi:10.1029/2001JB000482.
- Zlotnicki, J., and J. L. Le Mouél (1990), Possible electrokinetic origin of large magnetic variations at La Fournaise volcano, *Nature*, *343*, 633–636.
- Zonge, K. L., and L. J. Hughes (1991), Controlled source audio-frequency magnetotellurics, in *Electromagnetic Methods in Applied Geophysics—Applications*, vol. 2, edited by M. N. Nabighian and J. D. Corbett, pp. 713–809, Soc. of Explor. Geophys., Tulsa, Okla.

A. Maineult, Géomatériaux et Environnement, Institut de Physique du Globe de Paris, CNRS, and Université Paris VII—Denis Diderot, Tour 14, 4 place Jussieu, F-75005 Paris Cedex 05, France. (maineult@ipgp.fr)

J. Renner and E. Strobach, Institut für Geologie, Mineralogie und Geophysik, Ruhr-Universität Bochum, D-44780 Bochum, Germany.